Solvent volume dependent physical properties and electrocatalytic ability of nebulizer spray deposited CuInGaS2 counter electrode for dye-sensitized solar cells

C. Ravi Dhas, A. Jennifer Christy, R. Venkatesh, Subhendu K. Panda, B. Subramanian, K. Ravichandran, P. Sudhagar, A. Moses Ezhil Raj

PII: S0040-6090(18)30160-3
DOI: doi:10.1016/j.tsf.2018.03.017
Reference: TSF 36521

To appear in: *Thin Solid Films*

Received date: 22 December 2017
Revised date: 21 February 2018
Accepted date: 5 March 2018

Please cite this article as: C. Ravi Dhas, A. Jennifer Christy, R. Venkatesh, Subhendu K. Panda, B. Subramanian, K. Ravichandran, P. Sudhagar, A. Moses Ezhil Raj , Solvent volume dependent physical properties and electrocatalytic ability of nebulizer spray deposited CuInGaS2 counter electrode for dye-sensitized solar cells. The address for the corresponding author was captured as affiliation for all authors. Please check if appropriate. Tsf(2017), doi:10.1016/j.tsf.2018.03.017

Solvent volume dependent physical properties and electrocatalytic ability of nebulizer spray deposited $CuInGaS_2$ counter electrode for dye-sensitized solar cells

C. Ravi Dhas[1*], A. Jennifer Christy[1], R.Venkatesh[1], Subhendu K. Panda[2], B. Subramanian[2], K. Ravichandran[3], P. Sudhagar[4], A. Moses Ezhil Raj[5]

[1]PG & Research Department of Physics, Bishop Heber College (Autonomous), Tiruchirappalli-620 017, Tamil Nadu, India

[2]CSIR-Central Electrochemical Research Institute (CECRI), Karaikudi-630 006, India

[3]Department of Physics, AVVM Sri Pushpam College, (Autonomous), Poondi, Thanjavur-613 503, Tamil Nadu, India

[4]Photocatalyst and Coatings Group, SPECIFIC, College of Engineering, Swansea University (Bay Campus), Fabianway, Swansea, SA1 8EN, United Kingdom

[5]Department of Physics, Scott Christian College, (Autonomous), Nagercoil-629 003, Tamil Nadu, India

*Corresponding author email address: ravidhasc@gmail.com

Corresponding Author

Dr.C. Ravi Dhas
Head and Assistant Professor,
PG & Research Department of Physics,
Bishop Heber College (Autonomous),
Tiruchirappalli-620 017, Tamil Nadu, India.
Mobile: +91 9443076209
Land line: 0431-2770136
Fax: 0431-2770293
e-mail: ravidhasc@gmail.com; cravidhas@gmail.com

Abstract

$CuInGaS_2$ (CIGS) thin films were coated using nebulizer spray technique for different solvent volumes (10, 30, 50 and 70 ml) at the substrate temperature of 350 °C. The structural, optical and electrical properties were studied for the prepared CIGS thin films. CIGS thin films exhibited tetragonal structure and the maximum crystallite size was calculated for the film deposited using 50 ml solvent volume. The surface morphology of CIGS thin films was analyzed from scanning electron microscopy and atomic force microscopy studies. The electrical parameters of CIGS thin films such as resistivity, carrier concentration and mobility were examined using four probe method and Hall measurements. Electrocatalytic activities of the CIGS films towards redox couple (I^-/I_3^-) were analyzed by cyclic voltammograms, electrochemical impedance spectroscopy, and Tafel polarization measurements. The high photocurrent efficiency was obtained for the CIGS counter electrode prepared using 50 ml solvent volume.

Keywords: Thickness; Copper indium gallium sulfide; Nebulizer spray; Counter electrode; Dye-sensitized solar cells

1. Introduction

Environmental pollution, energy depletion and ecological destruction have prompted research on clean and renewable sources [1]. Recently, solar energy has been paid more attention to alternative non-renewable fossil sources [2]. Dye-sensitized solar cells (DSSCs) are promising new generation photovoltaic devices due to their low cost, ease of fabrication, high conversion efficiency and the ability to work under low light conditions compared to other solar cells (silicon) [3].

DSSC has three major components: a photoanode, an electrolyte with the redox couple (I^-/I_3^-) and a counter electrode (CE). In DSSCs, the CE plays a vital role, as it collects electron from the external source and reduces the redox couple process [4]. One of the most commonly used CE is Platinum (Pt) because of its high electrocatalytic behavior and electrical conductivity [5]. Conversely, Pt is expensive and less abundant which restricts its usage in large scale production [6]. To overcome the aforesaid, it is prerequisite to look for feasible CE with good electrocatalytic, stability and electrical conductivity. In recent days, many materials like conducting polymers, carbon materials, and the inorganic compounds have been proposed for an alternative Pt CE [3, 7].

Among inorganic compounds, chalcopyrite sulfides/ selenides like $CuInS_2$, $CuZnSnS_2$, $Cu_2ZnSnSe_4$, Cu_2FeSnS_4 etc., have been used as CE in DSSC [4, 8-10]. $CuInGaS_2$ (CIGS), which also belongs to chalcopyrite sulfide group, is a promising material for solar cell applications [11]. CIGS has been examined as an absorber layer for thin film solar cells due to its high absorption coefficient ($>10^5$ cm^{-1}) with the band gap energy value (1.5 eV) and has good stability [12, 13]. Yet, CIGS has not been explored more as a counter electrode in DSSCs. CIGS thin films have been prepared by various methods like co-evaporation [14], sputtering [15], electrodeposition [16], spray pyrolysis [11], etc. Nebulizer spray pyrolysis is a novel route to synthesis chalcopyrite thin films which has various advantages such as precise droplet control, simple engineering design, economical and has the ability to convert the precursor solution into aerosols [17]. Murakami et al. [18] have identified that thickness of the counter electrode layer has a decisive role in electron transfer for tri-iodide reduction. The thickness of the films plays a vital role in determining the morphology and electronic structure of a material. Recently our group has reported the nebulizer spray-deposited CIGS as a CE for different substrate temperatures [19]. In extension to that work,

the quantity of the $CuInGaS_2$ film deposited over fluorine doped tin oxide (FTO) needs to be optimized for effective electrocatalytic activity and photon to current conversion efficiency (η) in dye-sensitized solar cells.

In the present work, CIGS thin films were prepared by the nebulizer spray method at 350 °C for different solvent volumes. The effect of film thickness on structural, optical, and electrical properties was investigated. Further, CIGS was deposited on FTO substrate which was utilized as a counter electrode to analyze the performance of efficiency in dye-sensitized solar cells.

2. Experimental

2.1. Preparation of CIGS thin film

The principle and functioning of nebulizer spray unit had been reported previously by our research group [20]. The starting solution was prepared by dissolving copper (II) chloride dihydrate ($CuCl_2.2H_2O$), indium (III) chloride ($InCl_3$, anhydrous), gallium (III) chloride ($GaCl_3$, anhydrous) and thiourea ($SC(NH_2)_2$) in distilled water for different solvent volumes such as 10, 30, 50 and 70 ml with the molar ratio of 1:0.7:0.3:4. The obtained solution was stirred vigorously at room temperature and sprayed onto clean glass and FTO substrates at the optimized substrate temperature 350 °C [19]. The distance between the substrate and the nozzle is about 5 cm and the generated aerosols were transferred by the carrier gas with the pressure of 0.11 MPa and flow rate of 0.75 ml/ minute to produce device quality CIGS thin films.

2.2. Fabrication of DSSCs device

The TiO_2 blocking layer was spin coated over FTO substrates with 20 mM aqueous solution of $TiCl_4$ and annealed at 450 °C for 30 minutes. Using doctor blade method, the mesoporous and scattering TiO_2 layers were prepared and annealed at 500 °C for 1 h. The TiO_2 photoanode was dipped in 0.3 mM ethanolic solution of N719 dye for a period of 12 hours at room temperature. The ethanol solution was used to clean the excess amount of dye molecules present on the TiO_2 photoanode. 10 mM isopropanol solution of $H_2PtCl_6.6H_2O$ was employed to deposit Platinum CE on the FTO substrate using spin coating method. The obtained Pt CE was annealed at 400 °C for 30 minutes and used it for comparison. The prepared CIGS/FTO CEs for different solvent volumes and Pt CE were sandwiched with dye-sensitized TiO_2 by surlyn film. The active area of the fabricated DSSCs was 0.4 × 0.4 cm^2. The liquid electrolyte was prepared with acetonitrile using 0.06 M LiI, 0.6 M 1-propyl-2,3-dimethylimidazolium iodide, 0.03 M I_2, 0.5 M 4-tertbuyl pyridine and 0.1 M guanidinium thiocyanate and infused between the CIGS and TiO_2 electrodes to examine the photocurrent density – voltage study.

2.3. Characterization

The deposited CIGS films were characterized by X-ray diffraction patterns using a PANalytical X'PERT PRO diffractometer using Cu K_α radiation with a wavelength of 1.5406 Å. The Raman spectra were recorded by Reinshaw (Invia Make) spectrometer. The morphological studies were examined by Scanning Electron Microscope (Quanta 250FEG) and Atomic Force Microscope (A100, APE Research). Energy dispersive spectroscopy (Quanta 250FEG) was utilized to study the composition of the CIGS thin film. The optical absorbance spectra were detected from JASCO UV-Vis-NIR-V-670 Spectrophotometer. The electrical parameters of the prepared films were determined using Keithley 2400 and Ecopia HMS-3000 source meter. A solar

simulator (Photoemission Tech) with an AM 1.5G filter set was employed to record the photocurrent density – voltage measurements along with the potentiostat (VMP3, BIO-LOGIC) under illumination of 100 mW/cm^2. Cyclic voltammetry was measured under iodine electrolyte using Pt wire as counter electrode, standard calomel electrode (SCE) as reference electrode and CIGS/FTO served as working electrode. At a constant potential of 0.7 V with the frequency range between 0.1 Hz and 1 MHz and an amplitude voltage of 10 mV, the electrochemical impedance spectroscopy (EIS) study was investigated for the prepared samples under dark condition.

3. Results and Discussion

3.1. Thickness Measurements

The deposited film thickness was measured by stylus profilometer. The thickness of the coated CIGS thin films was increased non-linearly upto 50 ml which could be due to the nucleation and coalescence process taking place during the film growth [21] (Fig. 1). The decrease in film thickness at 70 ml causes the film formation to be powdery which is analogous to Shinde et al [22].

3.2. X-ray diffraction analysis (XRD)

The structural identification and changes in crystallinity of the CIGS thin films were analyzed by X-ray diffraction. The XRD patterns of CIGS thin film deposited for different solvent volumes are shown in Fig. 2. The film prepared at lower solvent volume (10 & 30 ml) exhibits amorphous nature due to incomplete formation of CIGS thin film. The peaks present at $2\theta = 28.2°$, 46.7° and 55.4° are indexed with (1 1 2), (2 0 4) and (2 1 5) planes respectively for the films deposited using 50 and 70 ml. X-ray photoelectron spectroscopy (XPS) analysis performed on 50 ml sample [19] confirmed the absence of CuS phase. The obtained peak values in the X-ray

diffraction pattern are in good agreement with tetragonal chalcopyrite CIGS (JCPDS card no. 65-1572). The plane (1 1 2) tends to grow with an increase in solvent volume and attained better crystallinity for the film deposited by 50 ml. The better crystalline nature is due to the increased ability of adatoms that occupy the exact site in the lattice [23]. The intensity of the peak decreased with further increase in the solvent volume (70 ml) as the thickness of the film decreased.

Scherrer's formula was used to examine the crystallite size (D) of the CIGS thin films:

$$D = \frac{K\,\lambda}{\beta \cos\theta} \qquad (1)$$

where 'K' is the shape factor (0.9), 'λ' is the wavelength of incident X-ray, 'β' is Full-Width Half Maximum (FWHM), 'θ' is diffraction angle**.** The microstrain (ε) and dislocation density (δ) of the CIGS thin films were estimated using the following equations,

$$\varepsilon = \frac{\beta \cos\theta}{4} \qquad (2)$$

$$\delta = \frac{1}{D^2} \qquad (3)$$

The crystallite size was calculated for the plane (1 1 2) and the maximum value (20 nm) was obtained for the solvent volume 50 ml with minimum dislocation density (2.45×10^{15} lines/m^2) and strain (1.17×10^{-3}). The larger crystallite size obtained for the solvent volume of 50 ml might be due to the increase in the deposition time that enhances more nucleation sites and the growth of the grains over the film surface [24]. The orientation effect probably disturbs the grain growth with further increasing the solvent volume (70 ml) which leads to minimum crystallite size

(17 nm) for the prepared film. From all the above observations, it is obvious that the solvent volume plays a crucial role in determining the quality of the CIGS thin film.

3.3. Raman spectra

Raman spectroscopy is used to analyze the vibrational mode of the thin film. Figure 3 (i) shows the typical Raman spectra of CIGS thin film for different solvent volumes. Generally, CIGS film has two structures, chalcopyrite (CH) and Cu-Au (CA) structures attributed to 290 and 305 cm^{-1}, respectively [25]. A narrow peak 296 and 298 cm^{-1} is observed for the CIGS film deposited using 50 and 70 ml, respectively and that peak indicates the mixture of both CH- and CA-structures. No other peaks related to impurity phases are observed indicating the purity of the deposited CIGS film. The higher FWHM (Fig. 3 (ii)) and shift of peak position at 311 and 304 cm^{-1} for the films deposited using 10 and 30 ml solvent volume could be attributed to the disorder owing to their poor crystalline nature as observed by X-ray diffraction [26]. The broadening of a peak (FWHM) is a sign to measure the degree of disorder present in the chalcopyrite system. The defect density is reduced remarkably as witnessed from the FWHM value (35 cm^{-1}) for the CIGS film deposited by 50 ml solution favorable for higher electrocatalytic activity in DSSC.

3.4. Scanning Electron Microscopy (SEM)

SEM images of CIGS thin film at different solvent volumes are depicted in Fig. 4. The solvent volume is one of the essential parameters in determining the morphology of the prepared thin films. The grains are small and non-homogeneously distributed as the droplet size resulting from the spray pyrolysis is tiny for 10 ml solvent volume. The grains begin to grow uniformly as

the solvent volume increases which can be elucidated based on the nucleation process involved in spray pyrolysis method. The sufficient amount of thermal energy at higher solvent volume develops a number of nuclei and produces larger grains due to lateral movement of grains [27]. Uniform distribution of larger grains is observed for 50 ml solution which is highly beneficial to efficient charge transfer in dye-sensitized solar cells. The films deposited at higher spraying quantities (70 ml) result in agglomeration due to the rich concentration of the solute.

3.5. Atomic force microscopy (AFM)

Typical two and three dimensional AFM micrographs are displayed in Fig. 5. The root mean square (RMS) roughness values of the CIGS thin film prepared for different solvent volumes is listed in Table 1. The surface roughness values decrease with the increasing solvent volume might be due to better uniform grain growth above 30 ml solution [28]. The growth of grains is restricted in CIGS film due to deficiency of the precursor at lower solvent volumes (10 & 30 ml) and hence resulting in the formation of smaller grains [29]. Figure 5 clearly presents the improvement in the surface morphology with the increase in solvent volume. The grains tend to grow in size and are uniformly distributed over the film surface (50 ml) and seem to be useful for large scale applications. Improvement in the grain size is essential because the small grain size of the film affects the diffusion length of the carriers and leads to low efficiency [23].

3.6. Energy dispersive X-ray spectroscopy (EDS)

Figure 6 shows EDS of CIGS film deposited for 50 ml solvent volume. The presence of elements such as copper, indium, gallium, and sulfur was confirmed. The inset of the table in Fig. 6 reveals better stoichiometric ratio for all the deposited CIGS thin films.

3.7. Electrical properties

The electrical conductivity and charge transport properties of CIGS thin films are essential for choosing the best counter electrode for dye-sensitized solar cells. The electrical parameters such as carrier concentration, mobility, and resistivity of the CIGS films for different solvent volumes were determined from four probe method and Hall effect measurements. All the CIGS films deposited by different solvent volumes exhibited positive Hall coefficient (R_H) value indicating the p-type behavior.

Temperature dependence of conductivity (ln σ vs 1000/T (K^{-1})) is given in Fig. 7 for the CIGS films deposited by different solvent volumes. The relation between temperature and dc conductivity can be expressed as

$$\sigma_{dc} = \sigma_0 \exp(-Ea / K_B T) \qquad (4)$$

where σ_0 is the pre-exponential factor, Ea is the activation energy and K_B is the Boltzmann constant. The plot can be divided into two regions (i) 303 – 370 K and (ii) 370 – 453 K and the activation energies (Ea_I & Ea_{II}) determined from the slope of the linear plot are listed in Table 1. The conduction mechanism in the first region could be due to the variable range hopping (VRH) conduction mechanism in which the charge transport occurs mainly due to the ions. The increase in conductivity from 370 – 453 K is dominated by thermionic emission of carriers [28]. The conductivity increases and the activation energy decreases with the increase in thickness of CIGS films, as the number of crystalline grain boundary decreases with an increase in grain size as observed from XRD results. The crystalline grain boundaries act as trapping centers which trap the majority charge carriers at the interface. Generally, in polycrystalline compound

semiconductors such as $CuInGaS_2$, the amorphous nature/random-oriented grains form potential barriers between grain-grain interfaces which strongly suppress the motion of the majority carriers [30]. The dependency of solvent volume on carrier concentration, resistivity and mobility is displayed in Fig.8. The increase in carrier concentration could be attributed to the improvement in crystalline nature and better grain growth with the increase in thickness. The variation in mobility values may be due to scattering during the charge transport by means of any one of the following scattering mechanisms such as (i) lattice or phonon vibrations (ii) grain boundary scattering (iii) scattering by impurity ions and grain boundary scattering [31]. CIGS thin films prepared by 50 ml solvent volume possess larger crystallite size which reduces the grain boundary regions thereby enhancing the electrical conductivity. The high carrier concentration with the considerable mobility of CIGS films prepared by 50 ml solvent volume could function as a better counter electrode in dye-sensitized solar cells.

3.8. Optical properties

A broad absorption spectrum covering the entire range of visible region is probably suited for solar cells. The absorption spectra of CIGS thin film deposited for different solvent volumes are shown in Fig. 9. The absorbance of CIGS thin films shows a sharp rise with increasing thickness. The decrease in absorbance for the film deposited at 70 ml could be attributed to the declining X-ray diffraction intensity. Notably, the maximum absorbance is obtained for the film deposited using 50 ml solution compared to other CIGS films.

The optical band gap energy of the CIGS thin film can be estimated using the Tauc plot relation [32],

$$\alpha h\nu = A\left(h\nu - E_g\right)^n$$

(5)

where 'α', '$h\nu$', 'E_g' and 'n' are absorption co-efficient, incident photon energy, band gap and type of transition. CIGS is a direct band gap semiconducting material (n=1/2)[33] and by extrapolating tangents to the 'X' axis, the optical energy band gap values of the deposited CIGS films (Fig.10) are observed to be 1.70, 1.61, 1.59 and 1.48 eV. The optical band gap values play a vital role in influencing the space charge region of solar cell devices.

3.9. Electrochemical activity and stability of CEs

The electrocatalytic activity of the CIGS CEs was evaluated by cyclic voltammetry (CV) with the three electrode system at a scanning rate of 50 mV/s. The solution was prepared by taking 10 mM LiI, 1mM I_2, and 0.1 M $LiClO_4$ and dissolved in the acetonitrile. Oxidation and reduction peaks were observed for all the CEs which indicate the redox couple (I^-/I_3^-):

$$3I^- \leftrightarrow I_3^- + 2e^- \quad (6)$$

Figure 11 (i) represents an anodic peak current density (J_{pa}) and a cathodic peak current density (J_{pc}) corresponding to the oxidation of I^- ions and the reduction of I_3^- ions. The current density and peak-to-peak separation (ΔE_p) were calculated to determine the electrocatalytic behavior of the CEs (Table 2). The current density values increases gradually with the increasing solvent volume which implies more catalytic behavior for thicker films. The maximum cathodic current density with the minimum peak-to-peak separation was obtained for the CIGS CE prepared by 50 ml compared to the other CEs. This indicates high electron transfer kinetics with better reversibility for the redox reaction I^-/I_3^- and hence this CE can be replaced with the expensive Pt CE in DSSCs. The improvement in the electrical conductivity and electrocatalytic activity results

in larger J_{pc}. Hence from CV analysis, we infer that high J_{pc} and low ΔE_p values would tend to higher short-circuit current density (J_{sc}) values of the DSSCs. The stability of the CIGS counter electrode prepared using 50 ml of solvent volume was examined continuously for 40 CV cycles in iodine electrolyte. From Fig. 11 (ii), the anodic and cathodic peak current densities of the CE seem to be identical which reveals better electrochemical stability in the (I^-/I_3^-) redox couple and also firmly attached on the FTO substrate.

3.10. Electrochemical Impedance Spectroscopy

To investigate the interfacial charge transfer and the kinetics of charge transport at the electrode/ electrolyte interface of CIGS and Pt electrodes, EIS measurements were carried out with TiO_2 based-DSSCs devices (Fig. 12 (i)). The series resistance (R_s) includes the sum of electrolyte resistance and the FTO resistance and R_{ct} corresponds to charge-transfer resistance at the counter electrode/electrolyte interface [34] and the estimated values are listed in Table 2. The equivalent circuit model for EIS curves was fitted using Zsimpwin software shown in inset Fig. 12 (i). The variation in R_s value of CIGS CEs could be attributed to the change in the electrical conductivity. Among the CIGS CEs, the lowest value of R_{ct} (14.90 (Ω cm^2)) is obtained for the CIGS CE prepared by 50 ml and signifying a better electrocatalytic property and a lower recombination at the interfaces. The decrease in R_{ct} value is highly efficient for charge transportation resulting in high efficiency in DSSCs.

3.11. Tafel Analysis

To understand the interfacial charge transfer of the CIGS symmetric cells, Tafel polarization measurements were performed. The electrocatalytic ability of counter electrode in tri-

iodide (I^-/I_3^-) reduction can be determined from the exchange current density (J_0) and the limiting diffusion current density (J_{lim}). From Fig.12 (ii), the value of 'J_{lim}' estimated from the intercept of Tafel polarization curves are listed in Table 2. The steepness of the slope in the anodic branch indicates high exchange current density. Both 'J_0' and 'J_{lim}' for CIGS CE deposited by 50 ml are comparable to that of Pt CE.

3.12. Photocurrent density-voltage (J-V) characterization

The photocurrent density-voltage curves of Pt and CIGS CEs under illumination are shown in Fig. 13 and the parameters determined from the curves are listed in Table 3. The decrement in the efficiency of CIGS CEs for lower thickness (10 & 30 ml) might be due to amorphous nature, poor electrical conductivity and weak bonding to the FTO substrate leads to poor electrocatalytic activity as reflected from CV studies. The DSSC of CIGS CE prepared for 50 ml exhibited highest DSSC efficiency of 4.32 % with open-circuit voltage (V_{oc}), short-circuit current density and fill factor (FF) being 0.77 V, 12.43 mA/cm^2 and 0.45, respectively. Under similar measurement conditions, the Pt CE displayed short circuit current density and efficiency of about 10.87 mA/cm^2 and 5.30 %. Even though the efficiency of CIGS CE is low compared to the Pt CE, the J_{sc} value of CIGS CE prepared by 50 ml solvent volume is higher than the Pt CE, and hence CIGS CE could substitute for Pt in future by improving some appropriate experimental conditions. In general, the series resistance and charge transfer resistance are crucial parameters in determining the fill factor in DSSCs [35, 36]. The CIGS film deposited using 50 ml solvent volume exhibited a high V_{oc} and J_{sc} but lower FF due to higher R_{ct} value (14.90 Ω cm^2) compared to Pt counter electrode (2.46 Ω cm^2) as observed from Nyquist plot (Fig.12 (i)). The R_s value of CIGS CE deposited using 50 ml solvent volume is low (4.15 Ω cm^2) compared to Pt CE (5.12 Ω cm^2) which shows the electron

transport from the external circuit for CIGS CE is faster but the higher R_{ct} value indicates electrocatalytic active sites are comparatively low for iodide complex reduction with Pt CE and thereby results in low FF. The limiting diffusion coefficient values of Pt and CIGS CE obtained from Tafel curve also supports our discussion. The η and J_{sc} for higher solvent volume (70 ml) dropped down to 2.47 % and 10.33 mA/cm^2. The reason for the decrement in J_{sc} could be attributed to high resistance for charge transport [35]. Larger grain boundaries lead to high resistance which in turn decrease electrical conductivity and hence photocurrent density [33]. The improvement of efficiency in the CIGS CE prepared for 50 ml results in low charge transfer resistance at the electrolyte/CE interface, fast reaction kinetics in the (I^-/I_3^-) redox couple and high electrocatalytic activity. These aspects are discussed in the aforesaid CV, EIS and Tafel sections. Compared to the other chalcogenides CEs, the high efficiency is obtained for CIGS CE prepared by cost effective nebulizer spray-coated technique for the better replacement of Pt CE [27, 35, 37, 38].

4. Conclusion

CIGS thin films were prepared for various solvent volumes using nebulizer spray technique. We observed that the structure, electrical and optical properties of the films are most sensitive to the film thickness. At lower solvent volumes, the films are in amorphous nature. The crystalline quality of CIGS thin films was improved with increase in solvent volume. The growth of grains was evenly distributed on the surface of the film deposited for the solvent volume 50 ml. The better electrical conductivity with higher carrier concentration was obtained for the film deposited by 50 ml. Evidentially the improvement in electrocatalytic activity and stability in the redox couple supported CIGS as an alternative CE. The photovoltaic properties of DSSCs for CIGS CEs were investigated. The highest efficiency of 4.32 % was achieved with the J_{sc} and FF

of 12.43 mA/cm^2 and 0.45 respectively for the film deposited by 50 ml. The present study reveals that the thickness of CIGS films plays a major part in disturbing the photovoltaic parameters. As a future work, the energy conversion efficiency of CIGS CEs has to be improved by tuning the other deposition conditions towards the replacement of conventional platinum counter electrode.

Acknowledgement

The authors would like to place on record their sincere thanks to the University Grants Commission, New Delhi for providing financial support through Major Research Project Scheme (MRP) [F.no.42-903/2013(SR)]. The authors also acknowledge Dr. R. Ramesh Babu, Assistant Professor, School of Physics, Bharathidasan University, Tiruchirappalli-24, for extending the Hall measurement facilities established under the DST grant (D.O.No.SR/S2/CMP-35/2004). One of the authors, Dr. S. K. Panda, would like to thank the Department of Science and Technology (DST), Government of India, for the financial support (Project no: SB/FT/CS-048/2012).

References

[1] B. He, Q. Tang, M. Wang, C. Ma, S. Yuan, Complexation of polyaniline and graphene for efficient counter electrodes in dye-sensitized solar cells: Enhanced charge transfer ability, J. Power Sources, 256 (2014) 8-13.
[2] K. Mokurala, S. Mallick, P. Bhargava, Alternative quaternary chalcopyrite sulfides (Cu 2 FeSnS 4 and Cu 2 CoSnS 4) as electrocatalyst materials for counter electrodes in dye-sensitized solar cells, J. Power Sources, 305 (2016) 134-143.
[3] H. Yuan, Q. Jiao, S. Zhang, Y. Zhao, Q. Wu, H. Li, In situ chemical vapor deposition growth of carbon nanotubes on hollow CoFe 2 O 4 as an efficient and low cost counter electrode for dye-sensitized solar cells, J. Power Sources, 325 (2016) 417-426.
[4] S.J. Yuan, Z.J. Zhou, Z.L. Hou, W.H. Zhou, R.Y. Yao, Y. Zhao, S.X. Wu, Enhanced Performance of Dye-Sensitized Solar Cells Using Solution-Based In Situ Synthesis and

Fabrication of Cu2ZnSnSe4 Nanocrystal Counter Electrode, Chemistry-A European Journal, 19 (2013) 10107-10110.
[5] L. Wang, M. Al-Mamun, P. Liu, Y. Wang, H.G. Yang, H.F. Wang, H. Zhao, The search for efficient electrocatalysts as counter electrode materials for dye-sensitized solar cells: mechanistic study, material screening and experimental validation, NPG Asia Materials, 7 (2015) e226.
[6] K. Mokurala, S. Mallick, Effect of annealing atmosphere on quaternary chalcogenide-based counter electrodes in dye-sensitized solar cell performance: synthesis of Cu2FeSnS4 and Cu2CdSnS4 nanoparticles by thermal decomposition process, RSC Advances, 7 (2017) 15139-15148.
[7] S.-L. Chen, A.-C. Xu, J. Tao, H.-J. Tao, Y.-Z. Shen, L.-M. Zhu, J.-J. Jiang, T. Wang, L. Pan, In situ synthesis of two-dimensional leaf-like Cu 2 ZnSnS 4 plate arrays as a Pt-free counter electrode for efficient dye-sensitized solar cells, Green Chemistry, 18 (2016) 2793-2801.
[8] X. Xin, M. He, W. Han, J. Jung, Z. Lin, Low-cost copper zinc tin sulfide counter electrodes for high-efficiency dye-sensitized solar cells, Angew. Chem. Int. Ed., 50 (2011) 11739-11742.
[9] J.-Y. Park, J.H. Noh, T.N. Mandal, S.H. Im, Y. Jun, S.I. Seok, Quaternary semiconductor Cu 2 FeSnS 4 nanoparticles as an alternative to Pt catalysts, RSC Advances, 3 (2013) 24918-24921.
[10] L. Wang, J. He, M. Zhou, S. Zhao, Q. Wang, B. Ding, Copper indium disulfide nanocrystals supported on carbonized chicken eggshell membranes as efficient counter electrodes for dye-sensitized solar cells, J. Power Sources, 315 (2016) 79-85.
[11] A. Kotbi, B. Hartiti, S. Fadili, A. Ridah, P. Thevenin, Some physical parameters of CuInGaS2 thin films deposited by spray pyrolysis for solar cells, Appl. Phys. A, 5 (2017) 1-8.
[12] W. Yao, Y. Wang, X. Wang, J. Zhu, Z. Zhang, X. Yuan, CuInS 2 thin films obtained by solid-state sulfurization, Mater. Sci. Semicond. Process., 26 (2014) 175-181.
[13] R. Kaigawa, D.M. Souza, Y. Satake, R. Klenk, Dependence of the Properties of Cu (In, Ga) S2/Mo Films Prepared by Two-Stage Evaporation Method on Degree of Vacuum during Deposition, Jpn. J. Appl. Phys., 51 (2012) 10NC17.
[14] R. Scheer, I. Luck, M. Kanis, M. Matsui, T. Watanabe, T. Yamamoto, Incorporation of the doping elements N and P in CuInS2 thin films by co-evaporation, Jpn. J. Appl. Phys., 39 (2000) 160.
[15] T. Watanabe, M. Matsui, Solar Cells Based on CuInS2 Thin Films through Sulfurization of Precursors Prepared by Reactive Sputtering with H 2S Gas, Jpn. J. Appl. Phys., 35 (1996) 1681.
[16] S.i. Kuranouchi, T. Nakazawa, Study of one-step electrodeposition condition for preparation of Culn (Se, S) 2 thin films, Sol. Energy Mater. Sol. Cells, 50 (1998) 31-36.
[17] P. Karthick, D. Vijayanarayanan, M. Sridharan, C. Sanjeeviraja, K. Jeyadheepan, Optimization of substrate temperature and characterization of tin oxide based transparent conducting thin films for application in dye-sensitized solar cells, Thin Solid Films, 631 (2017) 1-11.
[18] T.N. Murakami, M. Grätzel, Counter electrodes for DSC: application of functional materials as catalysts, Inorg. Chim. Acta, 361 (2008) 572-580.

[19] C.R. Dhas, A.J. Christy, R. Venkatesh, K. Anuratha, K. Ravichandran, A.M.E. Raj, B. Subramanian, S.K. Panda, Nebulizer spray-deposited CuInGaS 2 thin films, a viable candidate for counter electrode in dye-sensitized solar cells, Solar Energy, 157 (2017) 58-70.
[20] C. Ravidhas, B. Anitha, A.M.E. Raj, K. Ravichandran, T.S. Girisun, K. Mahalakshmi, K. Saravanakumar, C. Sanjeeviraja, Effect of nitrogen doped titanium dioxide (N-TiO2) thin films by jet nebulizer spray technique suitable for photoconductive study, J. Mater. Sci. - Mater. Electron., 26 (2015) 3573.
[21] U. Patil, K. Gurav, O.-S. Joo, C. Lokhande, Synthesis of photosensitive nanograined TiO 2 thin films by SILAR method, J. Alloys Compd., 478 (2009) 711-715.
[22] N. Shinde, R. Deokate, C. Lokhande, Properties of spray deposited Cu 2 ZnSnS 4 (CZTS) thin films, J. Anal. Appl. Pyrolysis, 100 (2013) 12-16.
[23] M. Öztas, Influence of grain size on electrical and optical properties of InP films, Chin.Phys.Lett., 25 (2008) 4090.
[24] V. Vani, M.V. Reddy, K. Reddy, Thickness-dependent physical properties of coevaporated Cu 4 SnS 4 films, ISRN Condensed Matter Physics, 2013 (2013) 1-6.
[25] M. Ajili, M. Castagné, N.K. Turki, Characteristics of CuIn 1− x Ga x S 2 thin films synthesized by chemical spray pyrolysis, J. Lumin., 150 (2014) 1-7.
[26] A. Jeong, W. Jo, M. Song, S. Yoon, Crystalline ordered states of CuIn 1− x Ga x Se 2 (x= 0, 0.3, and 1.0) thin-films on different substrates investigated by Raman scattering spectroscopy, Mater. Chem. Phys., 134 (2012) 1030-1035.
[27] S.S. Mali, P.S. Shinde, C.A. Betty, P.N. Bhosale, Y.W. Oh, P.S. Patil, Synthesis and characterization of Cu 2 ZnSnS 4 thin films by SILAR method, J. Phys. Chem. Solids, 73 (2012) 735-740.
[28] M. Sangamesha, K. Pushapalatha, G. Shekar, Effect of concentration on structural and optical properties of CuS thin films, International Journal of Research in Engineering and Technology, 2 (2013) 227-234.
[29] T.P. Rao, M.S. Kumar, N.S. Hussain, Effects of thickness and atmospheric annealing on structural, electrical and optical properties of GZO thin films by spray pyrolysis, J. Alloys Compd., 541 (2012) 495-504.
[30] F. Greuter, G. Blatter, Electrical properties of grain boundaries in polycrystalline compound semiconductors, Semicond. Sci. Technol., 5 (1990) 111.
[31] H. Cao, Z. Pei, J. Gong, C. Sun, R. Huang, L. Wen, Transparent conductive Al and Mn doped ZnO thin films prepared by DC reactive magnetron sputtering, Surf. Coat. Technol., 184 (2004) 84-92.
[32] C. Ravidhas, A. Juliat Josephine, P. Sudhagar, A. Devadoss, C. Terashima, K. Nakata, A. Fujishima, A. Moses Ezhil Raj, C. Sanjeeviraja, Facile synthesis of nanostructured monoclinic bismuth vanadate by a co-precipitation method: Structural, optical and photocatalytic properties, Mater. Sci. Semicond. Process., 30 (2015) 343-351.

[33] C. Ravi Dhas, A.J. Christy, R. Venkatesh, D.D. Kirubakaran, R. Sivakumar, K. Ravichandran, A.M.E. Raj, C. Sanjeeviraja, Effect of sputtering power on properties and photovoltaic performance of CIGS thin film solar cells, Mater. Res. Innovations, 21 (2017) 286-293.
[34] J.-G. Chen, H.-Y. Wei, K.-C. Ho, Using modified poly (3, 4-ethylene dioxythiophene): Poly (styrene sulfonate) film as a counter electrode in dye-sensitized solar cells, Sol. Energy Mater. Sol. Cells, 91 (2007) 1472-1477.
[35] Y.-F. Du, J.-Q. Fan, W.-H. Zhou, Z.-J. Zhou, J. Jiao, S.-X. Wu, One-step synthesis of stoichiometric Cu2ZnSnSe4 as counter electrode for dye-sensitized solar cells, ACS Appl.Mater.Interfaces, 4 (2012) 1796-1802.
[36] X. Xin, M. He, W. Han, J. Jung, Z. Lin, Low-Cost Copper Zinc Tin Sulfide Counter Electrodes for High-Efficiency Dye-Sensitized Solar Cells, Angew. Chem. Int. Ed., 50 (2011) 11739-11742.
[37] K. Mokurala, P. Bhargava, S. Mallick, Synthesis of Cu 2 ZnSnS 4 nanoparticles by solution based solid state reaction process and its application in dye sensitized solar cell as counter electrode, AIP Conference Proceedings, 1591 (2014) 1488-1490.
[38] S. Chen, A. Xu, J. Tao, H. Tao, Y. Shen, L. Zhu, J. Jiang, T. Wang, L. Pan, In-Situ and Green Method To Prepare Pt-Free Cu2ZnSnS4 (CZTS) Counter Electrodes for Efficient and Low Cost Dye-Sensitized Solar Cells, ACS Sustain.Chem.Eng., 3 (2015) 2652-2659.

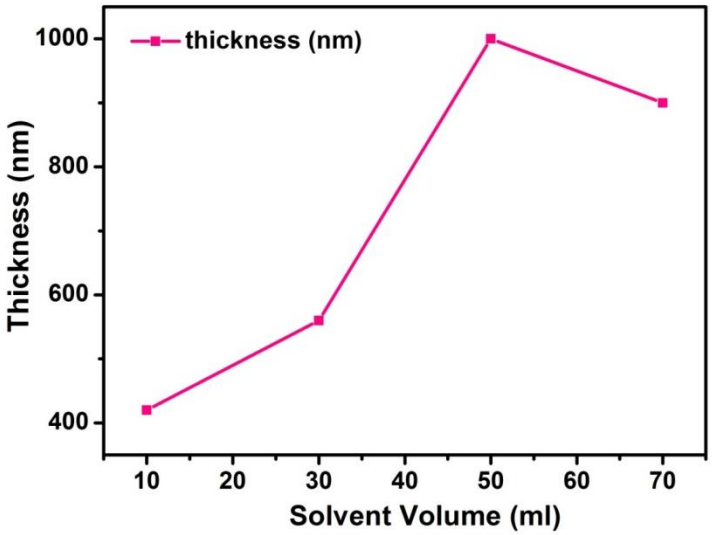

Figure 1: Variation of thickness with different solvent volumes

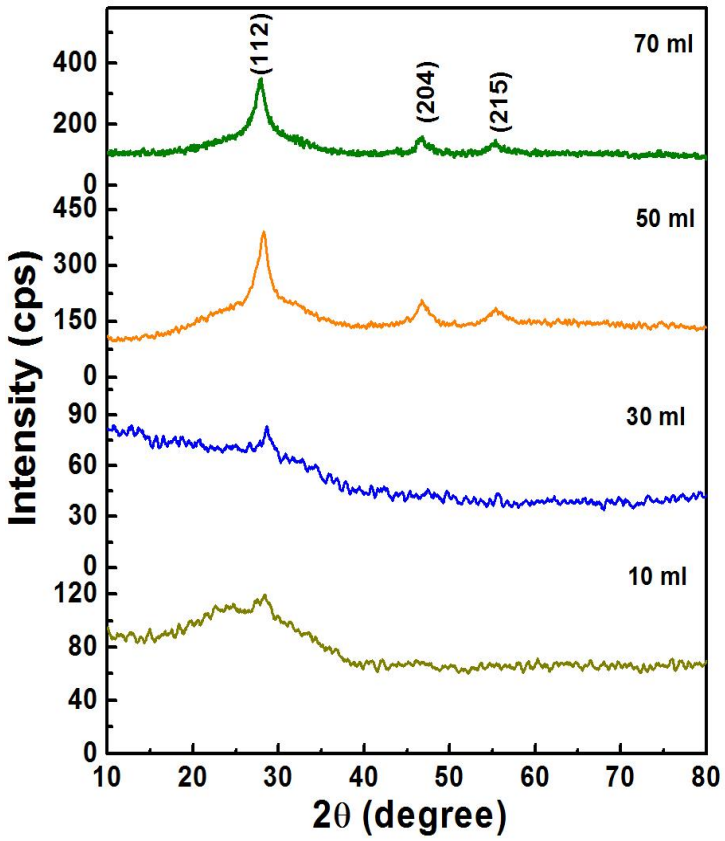

Figure 2: X-ray diffraction of CIGS thin films for different solvent volumes

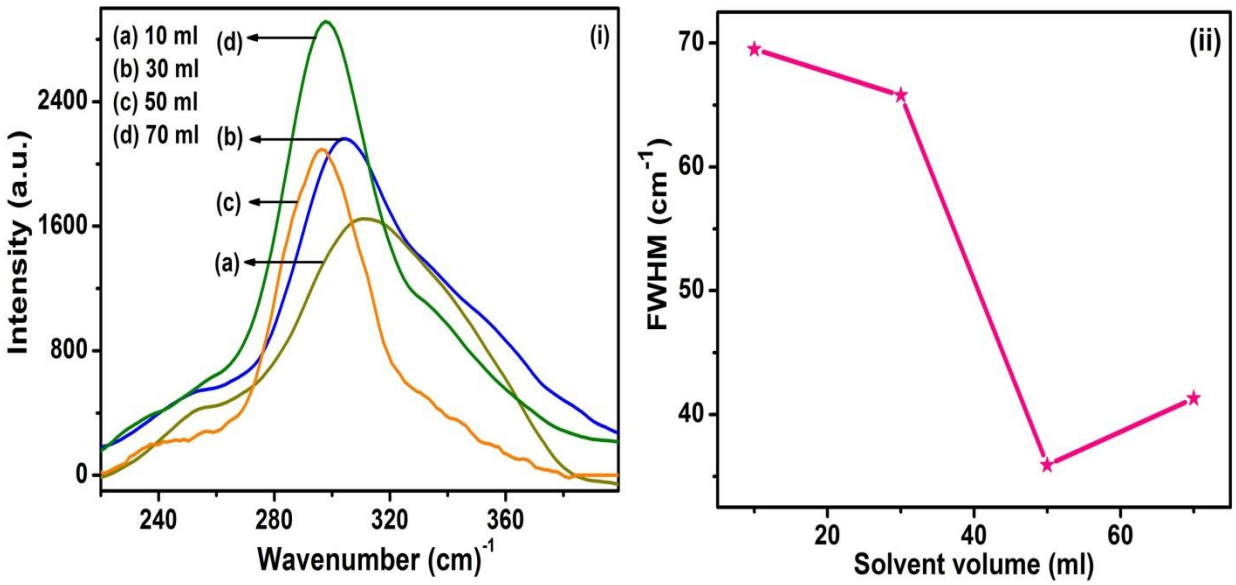

Figure 3: (i) Raman Spectra of CIGS thin films for different solvent volumes and (ii) Variation of FWHM with different solvent volumes

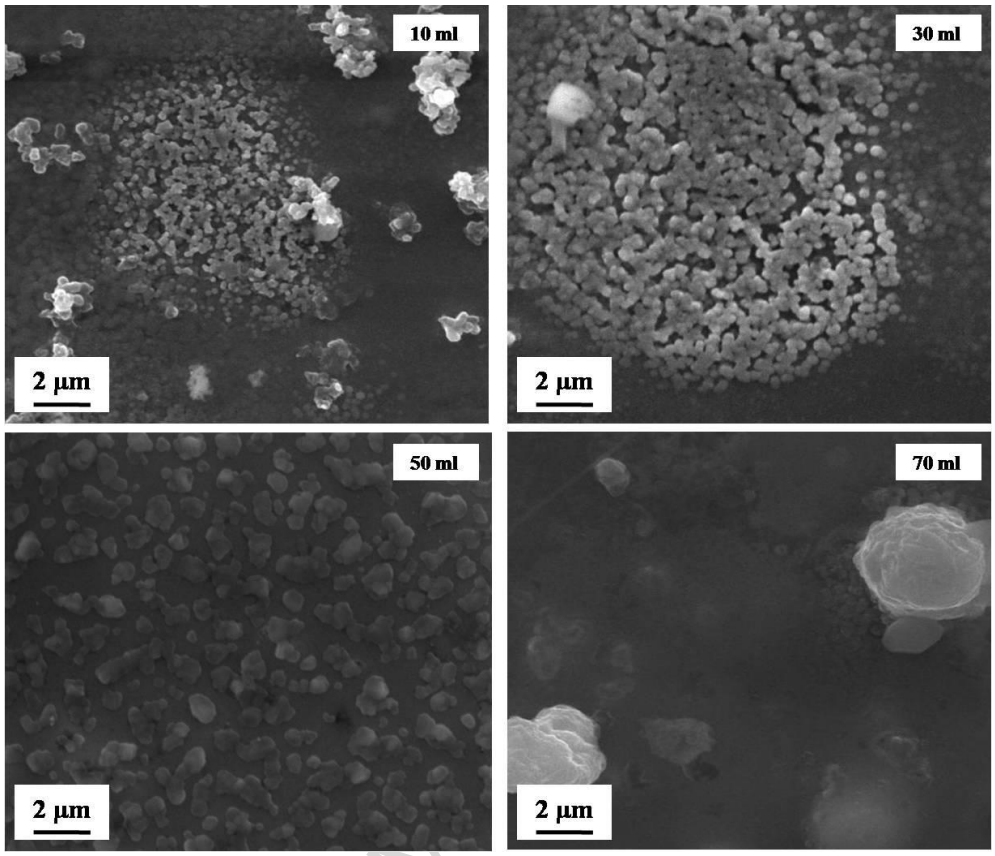

Figure 4: SEM images of CIGS thin film for different solvent volumes

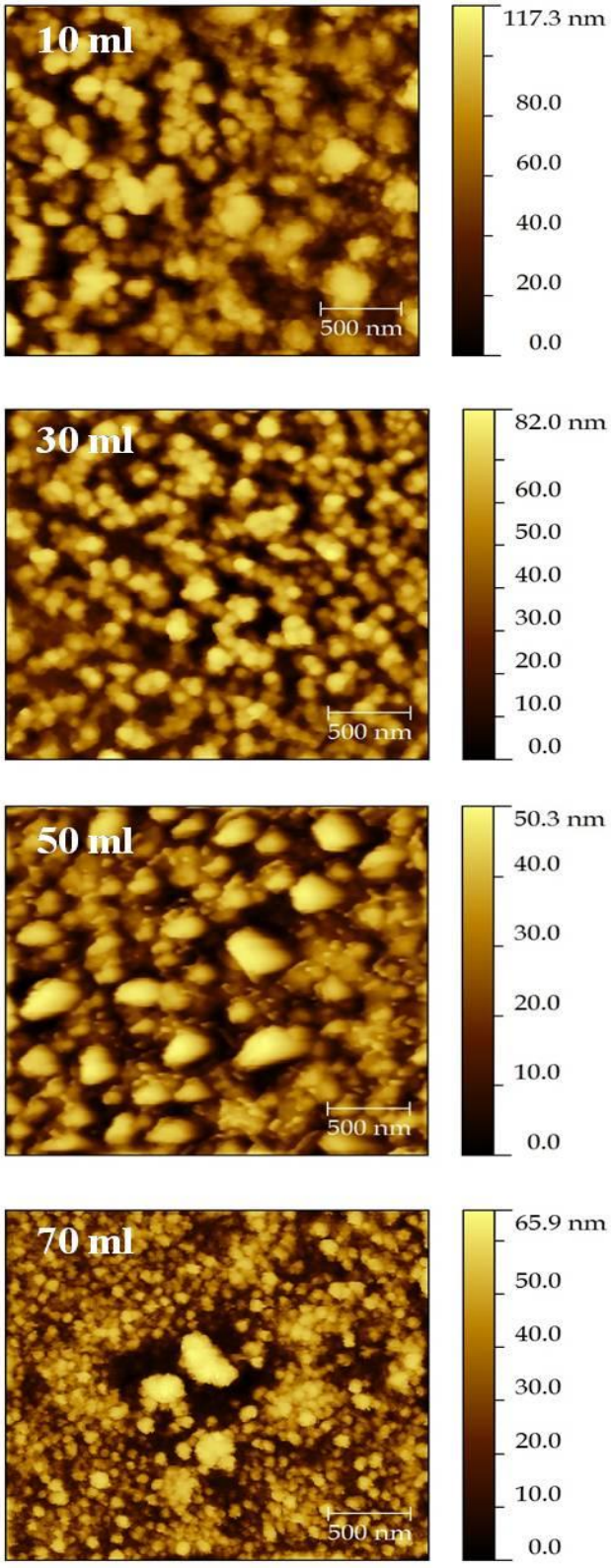

Figure 5: AFM images of CIGS thin film for different solvent volumes

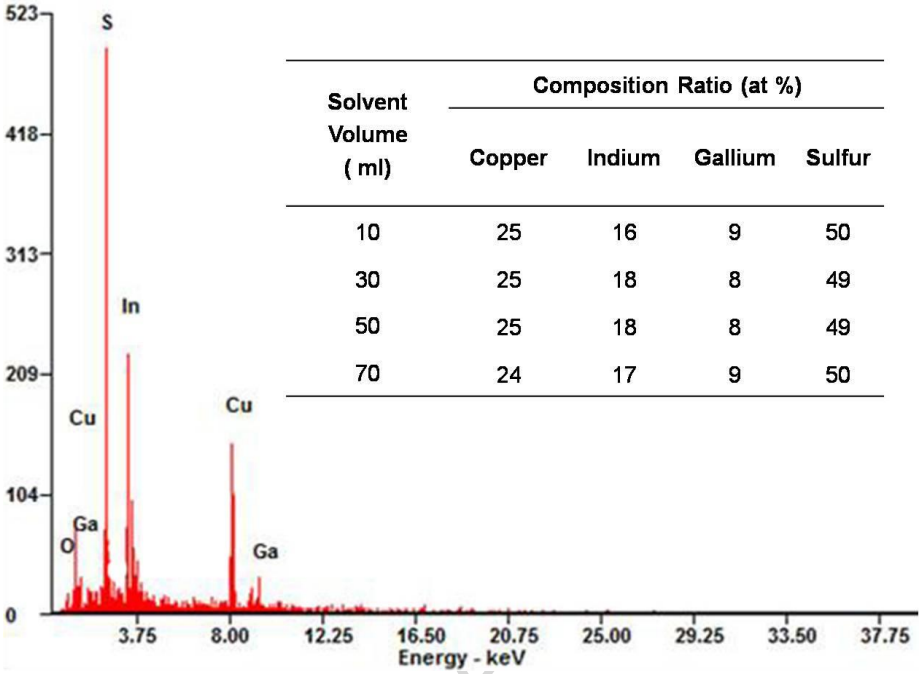

Solvent Volume (ml)	Composition Ratio (at %)			
	Copper	Indium	Gallium	Sulfur
10	25	16	9	50
30	25	18	8	49
50	25	18	8	49
70	24	17	9	50

Figure 6: EDS analysis of CIGS thin films

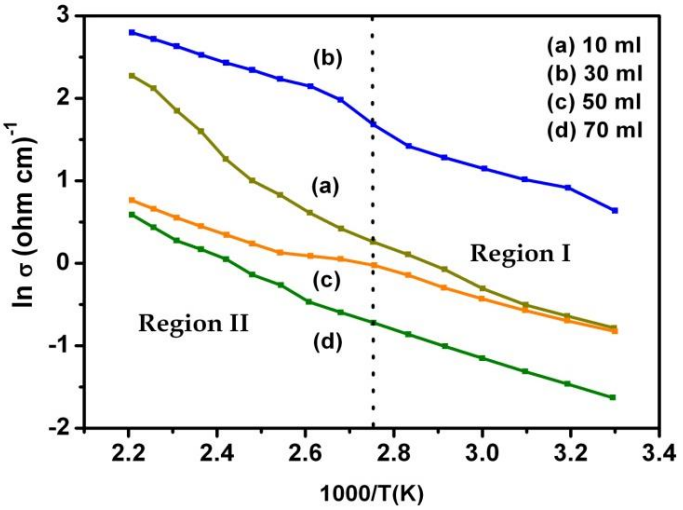

Figure 7: Arrhenius plot (ln σ vs. 1000/T (K^{-1})) of CIGS films for different solvent volumes

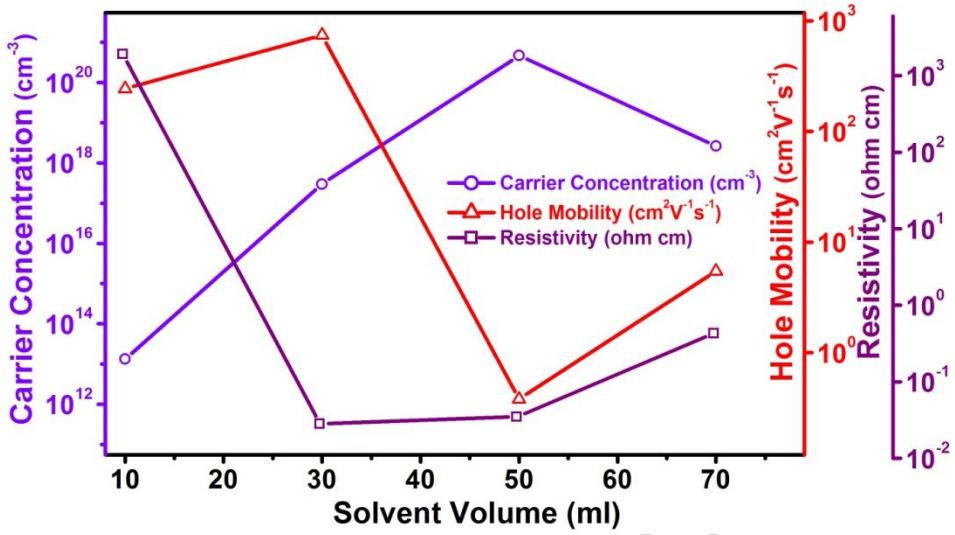

Figure 8: Electrical parameters of CIGS thin film for different solvent volumes

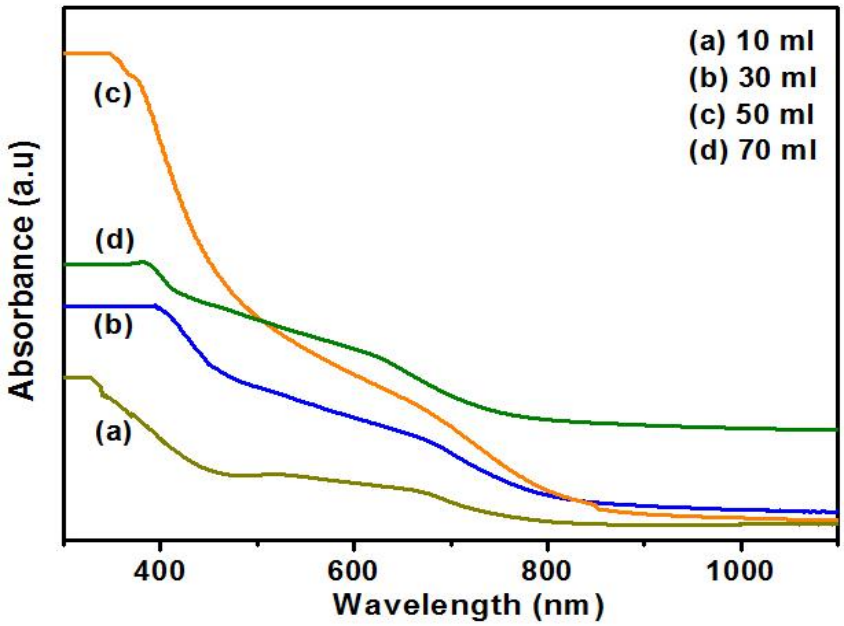

Figure 9: Absorbance vs wavelength of CIGS thin films for different solvent volumes

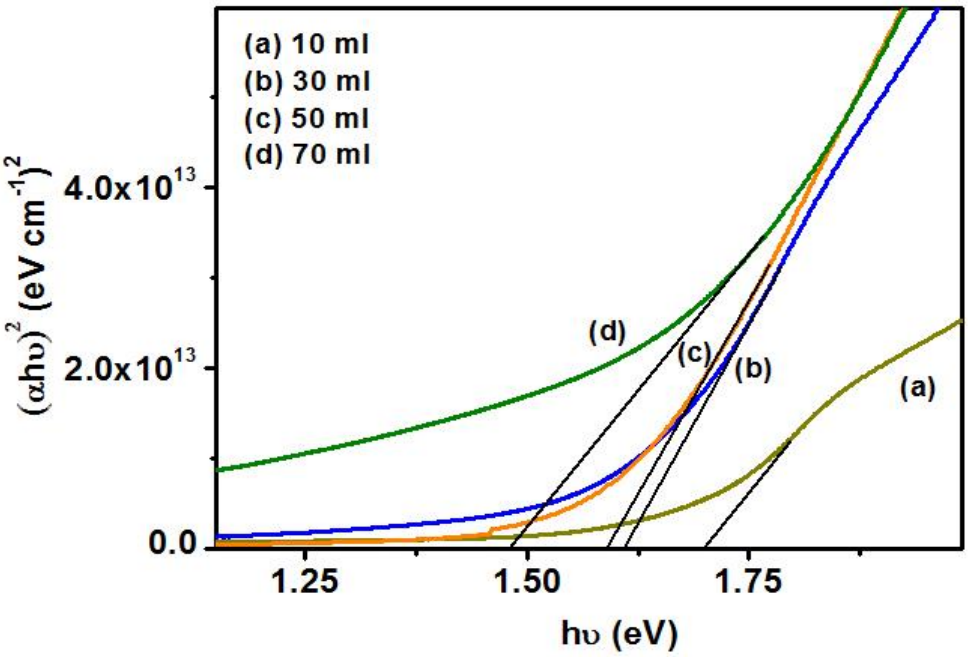

Figure 10: Optical band gap of CIGS thin films for different solvent volumes

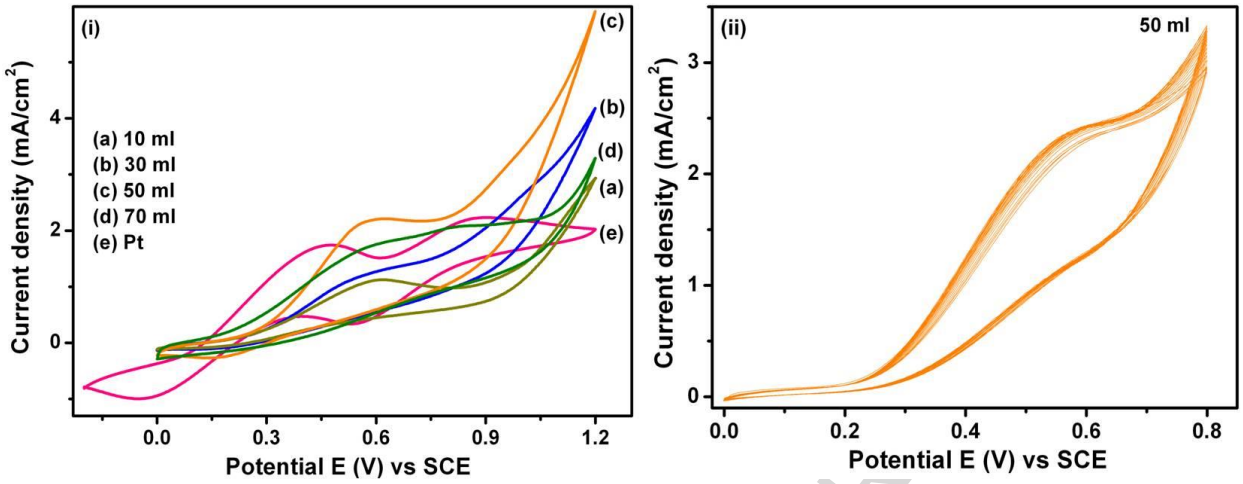

Figure 11: (i) Cyclic voltammograms of Pt and CIGS CEs and (ii) 40 continuous cyclic voltammograms of CIGS CE deposited for 50 ml

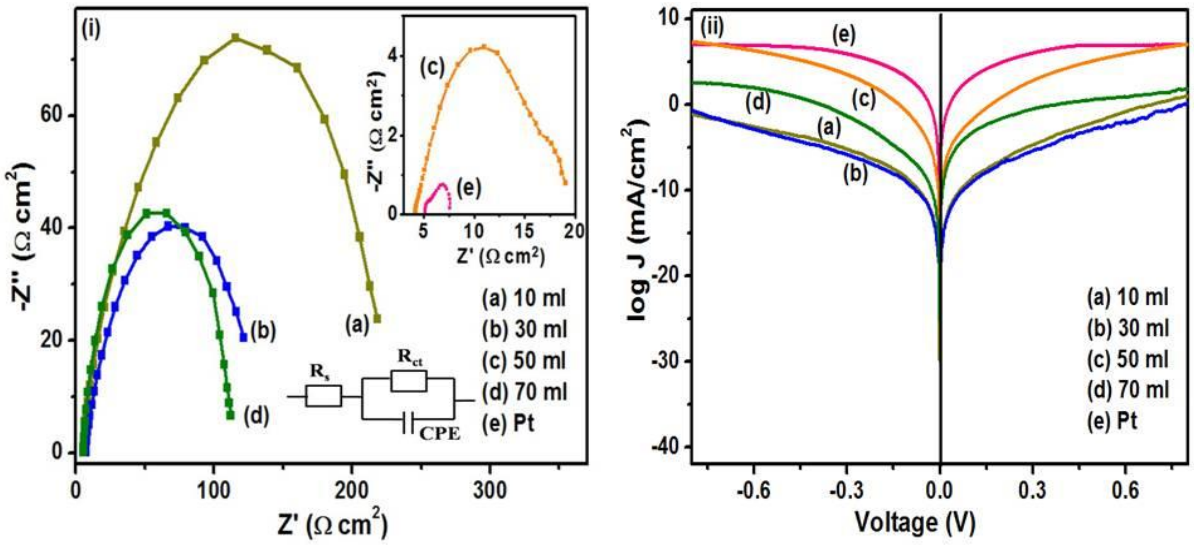

Figure 12: (i) EIS spectra of the TiO_2 based DSSCs devices with Pt and CIGS CEs and (ii) Tafel polarization curves of Pt and CIGS symmetric cells

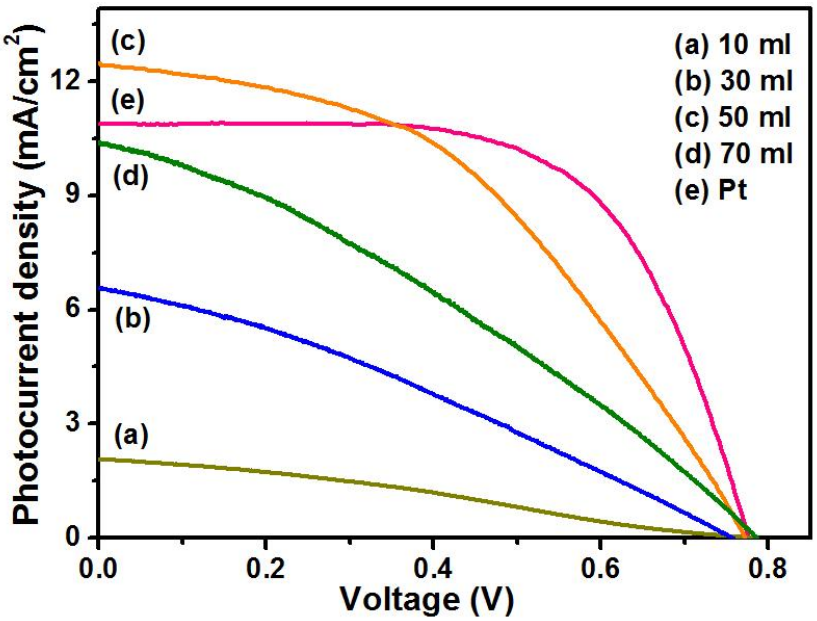

Figure 13: J – V characteristics of DSSCs with Pt and different CIGS CEs

Table 1: Root Mean Square Roughness and Activation Energy of CIGS thin films

Solvent Volume (ml)	Root Mean Square Roughness (nm)	Activation Energy (eV)	
		E_aI	E_aII
10	6.1	0.40	0.83
30	5.5	0.30	0.29
50	1.5	0.32	0.23
70	1.9	0.34	0.31

Table 2 Electrochemical parameters of DSSCs for different CEs

Samples	J_{pa} (mA/cm^2)	J_{pc} (mA/cm^2)	ΔE_p (mV)	R_s (Ω cm^2)	R_{ct} (Ω cm^2)	log J_{lim} (mA/cm^2)
Pt	1.75	-1.00	421	5.12	2.46	7.14
10 ml	1.12	-0.10	479	7.51	210.72	0.88
30 ml	1.21	-0.13	458	7.09	114.22	0.11
50 ml	2.20	-0.28	436	4.15	14.90	6.87
70 ml	1.68	-0.18	450	5.34	106.69	1.80

Table 3 Photocurrent density-voltage parameters of DSSCs for different CEs

Samples	V_{oc} (V)	J_{sc} (mA/cm^2)	FF	η (%)
Pt	0.78	10.87	0.63	5.30
10 ml	0.78	2.07	0.29	0.47
30 ml	0.76	6.54	0.30	1.47
50 ml	0.77	12.43	0.45	4.32
70 ml	0.79	10.33	0.30	2.47

Highlights

- Novel nebulizer spray technique is used for the deposition of $CuInGaS_2$ thin films.
- $CuInGaS_2$ thin films were used as counter electrodes in dye sensitized solar cells.
- Thickness effect on electrocatalytic ability of counter electrodes was studied.